Title: Distal axotomy enhances retrograde presynaptic excitability onto injured pyramidal neurons via trans-synaptic signaling

Authors: Tharkika Nagendran[1,3], Rylan S. Larsen[2,3,8], Rebecca L. Bigler[5], Shawn B. Frost[6,7], Benjamin D. Philpot[2,3,4], Randolph J. Nudo[6,7], Anne Marion Taylor[1,3,4]*

Affiliations:

[1] UNC/NCSU Joint Department of Biomedical Engineering, UNC-Chapel Hill, Chapel Hill, NC 27599 USA

[2] Department of Cell Biology and Physiology, UNC-Chapel Hill, Chapel Hill, NC 27599 USA

[3] Neuroscience Center, UNC-Chapel Hill, Chapel Hill, NC 27599 USA

[4] Carolina Institute for Developmental Disabilities, Chapel Hill, NC 27599 USA

[5] Curriculum in genetics and Molecular Biology Curriculum, UNC-Chapel Hill, Chapel Hill, NC 27599 USA

[6] Landon Center On Aging, University of Kansas Medical Center, Kansas City, KS 66160 USA

[7] Department of Rehabilitation Medicine, University of Kansas Medical Center, Kansas City, KS 66160 USA

[8]Present address: Allen Institute for Brain Science, Seattle, WA 98109, USA

*To whom correspondence should be addressed: amtaylor@unc.edu

Abstract

Injury of descending motor tracts remodels cortical circuitry and leads to enhanced neuronal excitability, thus influencing recovery following injury. The neuron-specific contributions remain unclear due to the complex cellular composition and connectivity of the CNS. We developed a microfluidics-based *in vitro* model system to examine intrinsic synaptic remodeling following axon damage. We found that distal axotomy of cultured rat pyramidal neurons caused dendritic spine loss at synapses onto the injured neurons followed by a persistent retrograde enhancement in presynaptic excitability over days. These *in vitro* results mirrored hyper-activity of directly injured corticospinal neurons in hindlimb motor cortex layer Vb following spinal cord contusion. *In vitro* axotomy-induced hyper-excitability coincided with elimination of inhibitory presynaptic terminals, including those formed onto dendritic spines. We identified netrin-1 as downregulated following axotomy and exogenous netrin-1 applied 2 days after injury normalized spine density, presynaptic excitability, and the fraction of inhibitory inputs onto injured neurons. These findings demonstrate a novel model system for studying the response of pyramidal circuitry to axotomy and provide new insights of neuron-specific mechanisms that contribute to synaptic remodeling.

Introduction

Acquired brain injuries, such as occur in stroke and traumatic brain injury, induce significant synaptic reorganization, even in uninjured cortical regions remote from the site of damage [1-3]. This enhanced neural plasticity supports formation of new connections and expansion of cortical territories, well-described in humans using neuroimaging and non-invasive stimulation techniques [1, 2, 4, 5]. However, the cellular mechanisms of this injury-induced plasticity remain largely unknown.

In healthy brains, long projection neurons with somatodendritic domains housed in cerebral cortex extend axons into numerous distant areas of the CNS, including the spinal cord and the apposing cortical hemisphere. When these remote areas are injured, long projection axons are damaged and injury signals propagate retrogradely to somatodendritic domains. Retrograde injury signal propagation leads to somatic responses such as chromatolysis and new transcription [6, 7]. For example, after damage to corticospinal axons resulting from spinal cord injury, dendritic spines in motor cortex undergo time-dependent changes in morphology including decreased spine density and alterations in spine length and diameter [8]. Loss of local GABAergic inhibition also occurs at somatodendritic regions following injury, which is thought to unmask preexisting excitatory connections and result in enhanced excitability [2, 9, 10]. These findings suggest that a cascade of events occurs following distal axonal injury involving retrograde axon-to-soma signaling and then trans-synaptic signaling from the injured neuron to uninjured presynaptic neurons causing synaptic changes and enhanced excitability.

Due to the heterogeneity and complexity of the CNS, intrinsic neuronal responses to distal axon injury and neuron-specific contributions to synaptic remodeling remain

unclear. Reduced preparations are valuable for examining these neuron-specific responses and provide a more experimentally tractable model system to identify and screen drugs to improve neuronal function following injury. Because brain injury and disease preferentially affect long projection neurons [11, 12], we sought to determine the progression of events that occur intrinsically in these neurons following distal axotomy leading to trans-synaptic changes. We overcame the technical challenge of visualizing and manipulating highly polarized and specialized cultured pyramidal neurons using a microfluidic approach.

Results

In vitro model to study distal axon injury to pyramidal neurons

To investigate how distal axon injury remodels synapses contacting injured neurons, we used a microfluidic approach to compartmentalize cultured pyramidal neurons. Using this approach we then subjected neurons to distal axotomy ~1 mm away from their physically undisturbed dendrites and somata [13, 14] (**Figure supplement 1a**). We used hippocampal neurons harvested from embryonic rats due to the ability to generate a relatively homogeneous, enriched population of pyramidal neurons (85-90% pyramidal) consistently from batch-to-batch, which exhibit morphology in line with maturing pyramidal neurons *in vivo* [15]; the remaining hippocampal neurons are mostly inhibitory GABAergic interneurons [16]. To identify neurons with axons projecting into the axonal compartment, we retrogradely labeled neurons by applying a G-deleted rabies virus expressing fluorescent proteins (incompetent for trans-synaptic transfer) to the axonal compartment and characterized the morphology of the labeled neurons. We found

that 94% (42 of 45) of virally-labeled neurons were pyramidal neurons and the remaining were unclassifiable (**Figure 1a**). When these neurons were cultured within the microfluidic chamber and axotomized within the axonal compartment (**Figure 1b**), the axotomized cultures showed no loss in viability post-axotomy (**Figure supplement 1**), similar to *in vivo* findings [17], and injured axons regrew [13, 14]. Supporting the use of this *in vitro* approach, we previously found that axotomy performed within the microfluidic chambers induced rapid expression of the immediate early gene *c-fos* [14], as reported *in vivo* [18]. Neurons labeled with retrograde tracer, Alexa 568-conjugated cholera toxin, also showed a significant decrease in Nissl staining in the somata reflective of chromatolysis at 24 h post-axotomy [19] (**Figure supplement 1**). Together, this *in vitro* model recapitulated key features of axotomy *in vivo,* and allowed us to examine the response of injured pyramidal neurons far from the site of injury.

Spine density decreases after distal axon injury

Decreased spine density is seen *in vivo* in models of traumatic brain injury and spinal cord injury [20, 21]. To determine whether similar structural changes occur in cultured pyramidal neurons following distal axotomy, we quantified spine density within the somatodendritic compartment of axotomized neurons that were retrogradely labeled using rabies mCherry virus. Spine density significantly declined 24 h and 48 h post-axotomy compared to before axotomy (**Figure 1c,d** and **Figure supplement 2**). In contrast, uninjured control neurons show increased spine density, as occurs during normal maturation (**Figure 1c,d)**.

We next analyzed specific spine types that were lost. We found a significant

decrease in the density of thin spines at 24 h post-axotomy compared to pre-axotomy (**Figure 2a**). The density of stubby and mushroom spines remained similar before and 24 h after axotomy, unlike in the uninjured control neurons where spine density of all spine types increased. At 48 h post-axotomy the density of both thin and mushroom spines was significantly reduced (**Figure 2a**). The reduction in spine density following axotomy suggests that either dendritic spines are being increasingly eliminated or, conversely, that there is a reduction in new spine formation following axotomy. Further analysis of our before and after axotomy images revealed that axotomy caused both a significant increase in the percentage of spines eliminated *and* a significant reduction in the percentage of new spines formed 24 h post-axotomy (**Figure 2b-d**). Thus, axotomy affects both elimination and formation of spines resulting in lower dendritic spine density.

A persistent enhancement in synaptic vesicle release rate follows distal injury

To further evaluate how synapses are modified following distal axon injury, we next investigated whether presynaptic release properties were altered at synapses onto injured neurons. To address this question, we retrogradely infected neurons using a modified eGFP rabies virus to label injured neurons and then used FM dyes to optically measure synaptic vesicle release onto these directly-injured neurons (**Figure 3a)**. The use of FM dyes provided us with a non-selective, unbiased method to label a majority of presynaptic terminals within the somatodendritic compartment [22]. FM puncta highly colocalized with synapsin1 immunolabeling (93%), validating our FM dye loading strategy (**Figure supplement 3**). We examined the synaptic vesicle release rate of FM puncta that colocalized with axotomized eGFP expressing neurons. At 24 h post-axotomy,

there was no change in synaptic vesicle release rate compared to eGFP expressing uninjured control samples (**Figure 3b,c**). In contrast, synaptic vesicle release rate was significantly enhanced 48 h after axotomy (**Figure 3c**). In addition, we found that the FM decay time constant, τ, which has been inversely correlated with release probability [23] was significantly reduced at 48 h post-axotomy (control: 138.3 s ± 8.761 versus axotomy: 88.62 s ± 5.132; $p<0.0001$). These results were similar to those obtained by examining the entire field of FM puncta near the barrier region without selecting only puncta that colocalize with eGFP expressing neurons (**Figure supplement 4**). The difference in presynaptic release rate persisted at 4 d post-axotomy (control: 88.3 s ± 1.43 versus axotomy: 82.3 s ± 1.552; $p=0.0046$; **Figure supplement 4**). Together, these data suggest a delayed and persistent increase in synaptic vesicle release rate that occurs following dendritic spine loss.

Next, we performed two control experiments to determine (1) whether cultured cortical neurons, which are more variable in neuron composition, would behave similarly to our pyramidal neuron-enriched hippocampal cultures used in our experimental model, and (2) whether axotomy of axons forming synapses onto postsynaptic targets would yield similar effects on presynaptic vesicle release as axotomy of untargeted axons. First, we performed FM unloading experiment with cortical neurons harvested from embryonic rats and found that these cultures show similar changes in presynaptic release 48 h post-axotomy (**Figure supplement 4**). To address the second question, we added a small number of target neurons to the axonal compartment during cell plating. We previously showed extensive synapse formation when two neuron populations are plated into opposing compartments [24]. By having a lower density of neurons in the target

153 compartment, there is negligible axonal growth into the barrier from these target neurons.
154 Our data show that axotomy to this targeted population of neurons resulted in similar
155 changes in presynaptic release rate as axotomy of untargeted axons (**Figure supplement**
156 **4**).

157 To reconcile our findings of axotomy-induced spine loss and increased
158 presynaptic release, we wondered whether the balance of responsive to unresponsive
159 presynaptic terminals was altered following axotomy resulting in enhanced excitability
160 even though fewer spines were present. We measured the proportion of FM puncta that
161 unloaded (responsive) or did not unload (unresponsive) in response to field stimulation
162 using extracellular electrodes [22] (**Figure 3d**). At 24 h post-axotomy when spine density
163 was decreased, we observed no change in the proportion of responsive and unresponsive
164 FM puncta compared to uninjured controls (**Figure 3d**). However at 48 h post-axotomy,
165 a significantly increased proportion of puncta were responsive compared to uninjured
166 control chambers (**Figure 3d**), suggesting enhanced presynaptic excitability at this time
167 point. Further, at 48 h post-axotomy we found a selective absence of unresponsive puncta
168 following axotomy while the total number of responsive FM-labeled puncta remained the
169 same (**Figure 3e**). Together, our data suggest that distal axon injury leads to an overall
170 decrease in quantity of presynaptic terminals, but that this smaller pool of presynaptic
171 terminals is more responsive to stimulation.

172

173 *Enhanced glutamate release occurs at synapses onto injured neurons*

174 Our results suggest that distal axotomy triggers a retrograde and trans-synaptic
175 cascade of events leading to enhanced neurotransmitter release. To confirm this, we

performed electrophysiological recordings of AMPAR-mediated miniature excitatory postsynaptic currents (mEPSCs) from axotomized neurons 48 h post-axotomy and their age-matched uninjured controls. Biocytin was used to fill neurons following each recording to determine whether neurons extended axons into the axonal compartment and were axotomized. Axotomized neurons had a significant increase in mEPSC frequency, supporting an increased rate of presynaptic glutamate release (**Figure 3f,g**). Membrane properties were equivalent between axotomized and uninjured control neurons, demonstrating that the health of these axotomized neurons was not substantially compromised (**Table supplement 1**). We observed a trend towards an increase in mEPSC amplitude following axotomy, however this effect was not significant (**Figure 3g**).

We next wondered if the increased spontaneous release rate of glutamate was specific to directly injured neurons or more globally affected neighboring, uninjured neurons. To address this, we quantified mEPSC frequency between uncut and cut neurons within the same chambers. In recordings from directly injured neurons, axotomy specifically increased mEPSC frequency. However, neighboring uninjured neurons that did not extend axons into the axonal compartment, did not have an increased mEPSC frequency (**Figure 3h**). To further examine the effects of direct injury to axotomized neurons, we quantified FM release rate at nearby uninjured neurons (not labeled with eGFP rabies virus) and found that the release rate was significantly different than at synapses on directly axotomized neurons and not significantly different than at control uninjured neurons labeled with eGFP rabies virus (**Figure 3i**). These observations confirmed that axotomy alters glutamatergic synaptic input onto injured neurons. These

199 results show that directly injured neurons transynaptically and locally influence
200 presynaptic glutamate release without affecting nearby synapses at uninjured neurons.

201

202 *Spinal cord injury (SCI) induces persistent and enhanced firing rates in layer Vb*

203 To evaluate the *in vivo* relevance of our findings, we sought to determine whether
204 distal injury of long projection neurons *in vivo* would preferentially induce enhanced
205 excitability in these injured neurons. To do this, we used a rat SCI model described
206 previously [25] in which animals were subjected to a spinal cord contusion injury at
207 thoracic level T9-10, and recording electrodes were implanted into the
208 neurophysiologically-identified hindlimb motor cortex in ketamine-anesthetized animals.
209 Electrode sites on single-shank microelectrode arrays (Neuronexus, Ann Arbor, MI)
210 extended through cortical layers V and VI, allowing simultaneous recording throughout
211 these cortical layers. Effective injury to the corticospinal neurons innervating hindlimb
212 motor neuron pools in the spinal cord was confirmed by stimulating electrode sites and
213 confirming loss of evoked hindlimb movement. At each cortical location, 5 minutes of
214 neural data was collected for offline analysis. At the end of the procedure, neural spikes
215 were discriminated using principle component analysis. We examined firing rates [26]
216 within layers Va, Vb, and VI between 4 weeks and 18 weeks post-SCI and compared the
217 data to sham control animals. We found that the firing rate within layer Vb was
218 significantly increased after SCI compared to sham controls (**Figure 4**). Layer Vb
219 contains the highest density of corticospinal somata, with estimates of nearly 80% of
220 large pyramidal cells [27]. Also, after spinal cord injury, chromatolytic changes occur
221 preferentially in layer Vb [28]. In layers Va and VI, which have few (layer Va) or no (layer

VI) corticospinal neurons, we found that firing rates were not statistically different between SCI animals and sham controls. Together, these data confirm a persistent increase in spontaneous firing rates in remotely injured corticospinal neurons, and support the relevance of our *in vitro* model system.

Axotomy selectively eliminates GABAergic terminals onto spines of injured neurons

Our *in vitro* data show that distal axon injury preferentially eliminated unresponsive presynaptic terminals to enhance the fraction of responsive puncta. Unresponsive presynaptic terminals may contain glutamate- or GABA- filled synaptic vesicles [29, 30]. Thus, we next asked whether the loss of unresponsive FM puncta correlated with loss of GABAergic puncta. We performed retrospective immunostaining to determine the fraction of vGLUT or GAD67-positive FM puncta at 48 h post-axotomy (**Figure 5a,b**). Interestingly, we found that axotomy did not alter the fraction of glutamatergic terminals, but significantly diminished the fraction of GAD67-positive puncta within the somatodendritic compartment. Thus our data suggest that distal axon injury induced a delayed enhancement in the fraction of responsive presynaptic terminals which may involve a reduction in the number of inhibitory terminals onto injured neurons, and not the number of excitatory presynaptic terminals.

To determine whether inhibitory synapses were functionally altered following axotomy, we recorded miniature inhibitory postsynaptic currents (mIPSCs) from axotomized and uninjured chambers 48h post-axotomy (**Figure 5c-e**). We found that mIPSCs were more frequent in axotomized cultures compared with uninjured neurons, suggesting that while there are fewer inhibitory terminals, the remaining terminals have

an increased rate of spontaneous GABA release. We next asked whether this change in inhibitory synapse function was restricted to directly injured neurons. Within the axotomized cultures, we compared both cut and uncut neurons and found that the mIPSC frequency was increased in both groups, but was not different between the directly axotomized neurons and their uncut neighbors. This suggests that the alteration of inhibitory synaptic transmission following axotomy affects both directly injured and neighboring, uninjured neurons.

Although the majority of GABAergic synapses are found on dendritic shafts or cell bodies, a minor population is also found on dendritic spines [31, 32]. Inhibitory synapses formed on dendritic spines allow for compartmentalization of dendritic calcium levels involved in regulation of neuronal activity [33, 34]. To investigate whether dendritic spines receiving inhibitory inputs (i.e., inhibited spines) are lost following axotomy, we quantified the number of inhibitory and excitatory presynaptic terminals onto spines of cultured pyramidal neurons subjected to distal axotomy compared to uninjured controls using retrospective immunostaining for inhibitory (vGAT) and excitatory (vGLUT) synapse markers. We found no significant difference in the fraction of vGLUT and vGAT-positive spines at 24 h post-axotomy compared to uninjured controls (**Figure 5)**. However, we noticed a significant decrease in the fraction of vGAT-positive spines at 48h post-axotomy compared to uninjured control (**Figure 5)** with no significant influence on glutamatergic spines. Together, our data suggest that axotomy causes a delayed loss of inhibitory synapses, an increase in spontaneous GABAergic transmission, and loss of inhibited spines coinciding with an enhancement in presynaptic excitability.

Local activity, retrograde signaling and differential gene expression regulate axotomy induced synaptic changes

Efficient axon regeneration requires signaling from the site of injury to the nucleus and transcription in multiple model systems [6], yet the signaling events required for synaptic remodeling following distal axotomy remain unclear. Breach of the axonal membrane following axon injury causes an influx of calcium and sodium ions into the intra-axonal space. An increase in sodium ions through voltage-gated sodium channels causes reversal of a sodium-calcium exchanger, and thus greatly enhances local intra-axonal calcium levels and potentially influences signaling to the nucleus and gene expression. To determine whether local influx of sodium and calcium ions at the time of injury is required for axotomy-induced spine loss, we performed axotomy within the axonal compartment in which axons were treated with a local activity blockade during axotomy. This local activity blockade solution (ABS) included low-Ca2+, high-Mg2+, and TTX (0.5 mM CaCl2, 10 mM MgCl2, 1 μM TTX) to prevent influx of sodium and reduce calcium influx. This local activity blockade was applied for 1 h during axotomy. We labeled neurons extending axons into the axonal compartment using a retrograde eGFP rabies virus and quantified spine density before and 24 h following axotomy and compared these measurements to cultures with vehicle applied to axons during axotomy (**Figure 6a,b**). Strikingly, we found that local activity blockade at the injury site prevented axotomy-induced spine loss. These data suggest that local activity instructs retrograde signaling and spine loss.

To determine whether injury-induced transcription is required for these trans-synaptic changes, we treated the somatodendritic compartment with the reversible

291 transcriptional blocker DRB 15 min prior to axon injury and removed the drug 45
292 minutes later. We found that blocking transcription during this brief time was sufficient
293 to prevent axotomy-induced spine loss 24 h post-axotomy (**Figure 6c**) and prevented
294 significant changes in the proportion of responsive FM puncta at 48 h post-axotomy
295 (**Figure 6d**). Transcription blockade also prevented changes in synaptic vesicle release
296 rate 48 h post-axotomy (**Figure 6e**). However, action potential blockade with TTX in the
297 somatodendritic compartment for ~1 h at the time of injury did not affect injury-induced
298 changes in presynaptic release or the proportion of responsive puncta (**Figure 6g,h**).
299 Further, application of HBS or DMSO as respective vehicle controls to TTX or DRB
300 treatments did not alter injury-induced increase in presynaptic release. We conclude that
301 both local activity at the site of injury and a transcriptional response are critical mediators
302 of the delayed trans-synaptic changes in presynaptic release properties following distal
303 axon injury.

304

305 *Differential gene expression at 24 h post-axotomy*

306 Our data show that a transcriptional response was required immediately after
307 axotomy to induce retrograde changes in synaptic vesicle release onto injured neurons.
308 To identify genes that might mediate this process within a longer therapeutically relevant
309 time window, we performed a gene expression study to identify differentially expressed
310 transcripts within the somatodendritic compartment at 24 h post-axotomy compared to
311 uninjured controls. We found 615 transcripts that were significantly changed following
312 injury (one-way between-subject ANOVA, $p < 0.05$) (**Figure 7a; Table supplement 1**).

313 Confirming that the transcription response *in vitro* recapitulated *in vivo* findings, we
314 found Jun upregulated 1.41 fold in our microfluidic cultures 24 h post-axotomy [17].

315

316 *Netrin-1 mRNA and DCC protein are down-regulated post-axotomy*

317 To identify potential trans-synaptic mediators that may influence synaptic vesicle
318 release at synapses onto injured neurons, we focused on differentially expressed
319 transcripts that are known to localize to cell-cell contacts, such as synapses (**Figure 7b**).
320 Within this category, only 6 transcripts were significantly changed. These transcripts
321 included Podoplanin (Pdpn), Kinesin family member 26B (Kif26b), Cadherin 24 - type2
322 (Cdh24), Myosin X (Myo10), Netrin1 (Ntn1) and Intercellular adhesion molecule2
323 (Icam2). We found that netrin-1 was significantly downregulated in our microarray study
324 and this was further confirmed by RNA-sequencing analysis of an additional set of
325 axotomized and uninjured neurons harvested from microfluidic chambers (unpublished
326 data). Netrin-1 is a secreted axon guidance and synaptogenic cue that is enriched at
327 mature dendritic spines [35] and is known to induce synaptic DCC clustering and enhance
328 synapse maturation [36]. Further, loss of secretory or trophic factors are known to induce
329 axotomy-like injury signals [37]. Because of the absence of suitable antibodies for
330 performing netrin-1 immunofluorescence, we tested whether its receptor, DCC, was
331 reduced following axotomy, as DCC levels parallel netrin-1 expression changes [38, 39].
332 While overall expression levels of DCC throughout the somatodendritic compartment
333 were unchanged, we found a significant decrease in local synaptic DCC
334 immunofluorescence at spines of axotomized neurons at 48 h post-injury (**Figure 8a,b**).
335 These data suggest that loss of netrin-1 in the somatodendritic compartment of

axotomized neurons may contribute to the trans-synaptic changes in neurotransmitter release.

Exogenous netrin-1 normalizes injury-induced enhancement in presynaptic excitability

To determine if netrin-1 could normalize the injury-induced enhancement in excitability, we applied exogenous netrin-1 to the somatodendritic compartment 40 h after-injury and evaluated the resulting changes in synaptic vesicle release and responsiveness compared to vehicle control at 48 h after injury. We found that application of exogenous netrin-1 normalized synaptic DCC levels to that similar to uninjured controls (**Figure 8a,b**). We tested whether exogenous netrin-1 treatment 40h post-axotomy might normalize spine density to levels quantified pre-axotomy. Impressively, we found that 8 h treatment with netrin-1 was sufficient to normalize spine density to pre-injury levels (**Figure 8c,d**). Further, exogenous netrin-1 increased the total number of FM puncta at 48 h post-injury to levels found in the uninjured control (**Figure 8e**). We also observed that application of netrin-1 for 8 h was sufficient to normalize injury-induced changes in the percentage of responsive puncta (**Figure 8f**). Further, netrin-1 treatment specifically led to the normalization of the number of vGAT puncta per neuron area without significantly altering the number of responsive or glutamatergic terminals, vGLUT puncta (**Figure 8g,h**). Together, our data suggests a novel role for netrin-1 in enhancing spine density, reducing injury-induced presynaptic hyper-excitability, and restoring the excitatory/inhibitory balance.

Discussion

We developed a model system to study the cellular mechanisms of synaptic remodeling following axon injury in long projection pyramidal neurons. Importantly, this *in vitro* model system recapitulates hallmarks of neurons subjected to axonal injury *in vivo*. These common hallmarks include chromatolysis [6, 19], retrograde spine loss [4, 20, 21], retrograde hyper-excitability [1-3], and disinhibition [2, 9, 10]. In addition, axotomy-induced transcriptional changes in this *in vitro* model are consistent with *in vivo* findings [7, 18]. This *in vitro* model system provides a unique tool to examine axotomy-induced retrograde signaling intrinsic to neurons and the resulting effects to interneuronal communication because of the simplified cellular environment and unprecedented access to neurons for both measurements and manipulations. Our study shows for the first time how changes in intrinsic properties of injured neurons influence presynaptic excitability across cells. This highly reliable *in vitro* system will likely be of great benefit for both basic research and drug discovery.

Our data show that synapses formed specifically onto directly-injured neurons have altered neurotransmitter release properties. Synapses onto uninjured neurons did not have such defects, suggesting that the trans-synaptic enhancement in excitability is localized at synapses forming onto injured-neuron during this time. Localized dendritic activity and activity-driven release of secreted proteins (e.g., BDNF, NT-3 and NT-4) from dendrites can trans-synaptically regulate neurotransmitter release [40, 41]. While the mechanisms that locally modulate neurotransmitter release remain unknown, netrin-1 signaling presents at least one potential route. Netrin-1 is secreted locally from target cells and signals DCC receptors that are present along axons [36], to influence presynaptic

terminal formation and maturation [42, 43]. Consistent with our findings, netrin family members were downregulated *in vivo* following spinal cord injury in adult rats [44, 45] and DCC remained persistently low after 7 months post-injury in adult rats [44]. Netrin-1 has also been tested as a potential therapeutic agent following injury and has been shown to improve recovery outcomes [46-48]. Our results suggest, for the first time, that netrin-1 may play a critical role in regulating inhibition loss following injury.

We found a significant reduction in the fraction of inhibitory terminals onto injured neurons 48h post-axotomy. This data together with the persistent loss in spine density post-axotomy, lead us to hypothesize that axotomy induces a specific loss of inhibited spines. Our data showed this was indeed the case. This finding is significant because it suggests a new role for the often-ignored inhibitory spines (~10% of spines in our cultures) [31, 32]. It also suggests that excitatory inputs are spared at least for some time following axotomy. Specific loss of inhibitory and not excitatory terminals suggests that retracted excitatory inputs could form new connections while inhibitory ones disappear early after axotomy. It is also possible that large head dendritic spines could receive multiple excitatory inputs suggesting that these terminals are stable and could find new partners over time after injury.

Our results showing down-regulation of netrin-1 post-axotomy are consistent with *in vivo* findings following spinal cord injury [44]. Netrin-1 is known to enhance presynaptic terminal formation and maturation [42, 43], thus the loss of netrin-1 following distal injury may have an opposite effect, causing presynaptic terminals to become more functionally immature. Our data supports this conclusion, as we found that presynaptic inputs onto injured pyramidal neurons exhibited a reduced recycling synaptic vesicle pool size and

404 increased release rate, both associated with immature terminals [49, 50]. Further, we found
405 that application of exogenous netrin-1 normalizes the injury induced decrease in synaptic
406 levels of DCC and the immature-like hyper-excitability (**Figure 8)**. Since netrin-1 and
407 DCC are enriched at glutamatergic synapses within the mature mammalian brain [35], these
408 results point to netrin-1 as a promising therapeutic target to address excitability post-
409 injury. Other trans-synaptic signaling targets (**Figure 7b)** may also influence intrinsic
410 neuronal excitability following brain injury and stroke. Our microfluidics-based model
411 system provides a scalable platform to examine the influence of these and other targets on
412 synaptic remodeling of pyramidal neurons following distal injury.
413

414 **Materials and Methods**

415 **Materials and Methods**

416 *Hippocampal cultures.* Dissociated hippocampal cultures were prepared from
417 Sprague Dawley rat embryos (E18-E19) as previously described [14, 22] with the following
418 modifications. Hippocampal tissue was dissected in dissociation media (DM) containing
419 82 mM Na_2SO_4, 30 mM K_2SO_4, 5.8 mM $MgCl_2$, 0.25 mM $CaCl_2$, 1 mM HEPES, 20 mM
420 Glucose and 0.001% Phenol red. For enzymatic digestion, equal volumes of TrypLE
421 Express (Invitrogen) and DM were added to the tissue and incubated at 37°C for 8 min.
422 Tissue was then rinsed and gently triturated in neuronal culture media consisting of
423 Neurobasal media (Invitrogen) supplemented with 1x B27 (Invitrogen), 1x Antibiotic-
424 antimycotic (Invitrogen), 1x Glutamax (Invitrogen). Dissociated cells were resuspended
425 in neuronal culture media to yield $12x10^6$ cells per ml.
426

427 *Microfluidic chambers.* Poly(dimethylsiloxane) (PDMS) microfluidic chambers
428 were replica molded from microfabricated master molds as described previously [14]. All
429 experiments used chambers with 900 µm long microgrooves to separate the
430 somatodendritic and axonal compartments as described previously [13, 14, 22]. Microfluidic
431 chambers were placed onto glass coverslips coated with 500-550 kDa Poly-D-Lysine
432 (BD Biosciences). Approximately ~90,000 cells were plated into the somatodendritic
433 compartment and axons extended into the adjacent axonal compartment after 5-7 days of
434 culture. Axotomy was performed at 13 days in vitro (DIV) as described previously [13, 14].
435
436 *Retrograde labeling.* Retrograde labeling was performed using either modified
437 cholera toxin or rabies virus. Cholera Toxin Subunit B Alexa Fluor 488 or 568 (Life
438 technologies, Molecular Probes; 1 µg in 200µl of neuronal culture media) was added to
439 the axonal compartment of the microfluidic chamber and incubated for ~ 15h at 37°C.
440 After 15h of incubation, the axonal compartment media was removed, rinsed and
441 replaced using fresh neuronal culture media before performing axotomy or imaging.
442 G-deleted Rabies-mCherry or GFP virus [51] (Salk Institute; $1x10^5$ viral units) in 50
443 µl- conditioned media was added to the axonal compartment of each chamber and
444 incubated for 2h at 37°C. Conditioned media was added back to the axonal compartments
445 following two washes with fresh NBE media. Chambers were maintained in 37°C
446 incubator for ~48 h until fluorescence expression was visible.
447
448 *Cell viability assay.* Dead cells were labeled using SYTOX Green (Invitrogen) at
449 a final concentration of 1 µM and all cell nuclei were labeled with NucBlue Hoechst

450 Stain (Invitrogen). Cells were incubated with SYTOX/Hoechst solution simultaneously in
451 1x PBS for 5 min at 37°C, washed with PBS, and fixed with 4% paraformaldehyde (PFA)
452 in PBS containing 40mg/ml sucrose, 1 µM $MgCl_2$ and 0.1 µM $CaCl_2$ for 15 min at room
453 temperature (RT). Coverslips were then rinsed three times with PBS and mounted onto
454 the glass slide using Fluoromount G (Southern Biotech). SYTOX positive ($Sytox^+$) cells
455 were manually counted in ImageJ using sum projected z-stack confocal images. Percent
456 cell viability is calculated using [($Sytox^+$ - Hoechst) / Hoechst] * 100.
457
458 *Nissl Staining.* Neuronal cultures retrogradely labeled with Cholera Toxin were
459 either axotomized or left uninjured. PDMS chambers were carefully lifted off from PDL
460 coated coverslips 24 h post-axotomy. Cultures on the coverslips were quickly rinsed
461 twice with PBS, fixed with 4% PFA for 30 min at RT, washed twice in PBS, and
462 incubated in 0.1% Triton X-100/PBS for 10 min at RT. Cultures were incubated for 20
463 min in NeuroTrace 500/525 Green Fluorescent Nissl Stain (1:100; Invitrogen) and
464 washed for 10 min in 0.1% Triton X-100/PBS. Cell nuclei were stained with DAPI
465 (Sigma-Aldrich), rinsed three times in PBS, and then the coverslip was mounted onto a
466 microscope slide using Fluoromount G.
467
468 *Immunocytochemistry.* PFA fixed neuronal cultures were permeabilized in 0.25%
469 Triton X-100 and blocked in 10% normal goat serum for 15 min each. Coverslips were
470 incubated with anti-MAP2 (1:1000; Millipore), anti-beta tubulin III (1:2000;Aves), anti-
471 GAD67 (1:2000; Aves labs, GAD), anti-vGLUT1 (1:100; NeuroMab), anti-vGAT
472 (1:1000; Synaptic Systems), anti-DCC (1:100; Calbiochem), or anti-synapsin1 (1:500;

Calbiochem) primary antibodies in 1% blocking solution for overnight at 4°C. Coverslips were then incubated with goat anti-rabbit or goat anti-mouse or anti-chicken secondary antibodies conjugated to Alexa-fluorophores (1:1000; Invitrogen) for 1h at RT. Following PBS washes coverslips were mounted onto the glass slide.

RNA isolation. Total RNA from each of 3 axotomized devices and 3 sham manipulated devices (6 total samples) was isolated from the somatodendritic compartment of DIV14 cultures, 24 h after manipulation, using the RNAqueous-Micro Kit (Ambion) according to the manufactures instructions including DNase treatment, with modifications specific to accessing the microfluidic compartment [13]. Briefly, 50 µl lysis solution was added to one somatodendritic well and collected from the other somatodendritic well. Lysate was added to 50 µl of fresh lysis solution and mixed well by careful pipetting. Further RNA purification steps were performed according to the manufacturer's guidelines. Samples were maintained at -80ºC until prepared for microarray gene expression.

Microarray analysis. Quantification of RNA integrity and concentration was confirmed with an Agilent TapeStation 2200 at the UNC Lineberger Comprehensive Cancer Center Genomics Core. Microarrays were processed at the UNC School of Medicine Functional Genomics Core using the Affymetrix GeneChip WT Plus Reagent Kit for cRNA amplification, cDNA synthesis, fragmenting and labeling. Samples were hybridized to Rat Gene 2.0 ST Arrays (Affymetrix). Data analysis was performed with Affymetrix Expression Console software and Affymetrix Transcriptome Analysis

Console v2.0 software to compare axotomized cultures to uninjured control samples using one-way between-subject ANOVA of normalized intensities. We defined our list of significantly changed transcripts as having a fold change absolute value ≥ 1.1 and an ANOVA p-value <0.05. To further identified cell-cell adhesion transcripts by searching for the biological process gene ontology category 'cell-cell adhesion'. Fold-change was calculated by dividing the mean log_2 intensity value of the uninjured control by the mean log_2 intensity value of the axotomized culture samples. The microarray data will be submitted to GEO and accession numbers will be provided at the time of publication.

Image acquisition and dendritic spine analysis. High-resolution z-stack montages of mCherry or GFP labeled live neurons were captured using Zeiss LSM 780 (63x 1.4 NA or 40x 1.4 NA oil immersion objective). Fluorescently labeled fixed neurons (**Figure 2- figure supplement 2)** were captured using Olympus IX81 microscope (60x 1.3 NA silicon oil immersion objective). To track axotomy induced changes, mCherry labeled 24 h post-axotomy cultures and those uninjured were fixed with 4%PFA for 30 min RT. Dendrite and spine measurements from montages of fixed (**Figure 2- figure supplement 2**) or live neurons were analyzed as described below. In live imaging, we captured " 0 h or before axotomy" confocal z-stack images using a 40x and 63x objective to create montages of neurons extending axons into the axonal compartment. Axotomy was performed on the same day after acquiring these images. Images were acquired from same neuron 24 h post-axotomy. In some cases, images were also acquired from same neurons at 48 h post-axotomy (Figure1, 2 and 8). Calibrated z-stack montages were analyzed for all dendrite and spine parameters. Dendrites were traced

519 using semiautomatic neurite tracing tool, Neuron J [52, 53]. Dendrites greater than 10 μm in
520 length were used in the analysis and were quantified for total dendrite length and number
521 of branch points (total number of dendrites - number of primary dendrites). Number of
522 spines on all primary dendrites of each neuron were manually labeled and categorized as
523 thin, stubby or mushroom shaped based on each spine's head to neck diameter ratio (neck
524 ratio) and length to head diameter ratio using Neuron studio [54]. Spine density was
525 calculated for 10 μm length of dendrite as [(# of spines / dendrite length)*10].
526
527 *FM dye experiments and analysis.* Cultures in microfluidic chambers at 24 h
528 (14DIV), 48 h (15DIV), and 4d (17DIV) post-axotomy were loaded with lipophilic dye
529 FM® 5-95 (Invitrogen) using KCl mediated depolarization as described previously [22].
530 Briefly, culture were first incubated for 30 min with pre-warmed HEPES-buffered
531 solution (HBS; 119 mM NaCl, 5 mM KCl, 2 mM $CaCl_2$, 2 mM $MgCl_2$, 30 mM glucose,
532 10 mM HEPES). Media was then replaced with FM dye loading solution containing
533 10 μM FM 5-95, 20 μM AMPAR antagonist 6-cyano-7-nitroquinoxaline-2,3-dione
534 disodium (CNQX; Tocris), 50 μM NMDAR antagonist D-(-)-2-amino-5-
535 phosphonopentanoic acid (D-AP5; Tocris) in 90 mM KCl HBS for 1 min. The loading
536 solution was replaced with HBS containing 10 μM FM 5-95 for 1 min and later rinsed
537 three times with a high-Mg^{2+}, low-Ca^{2+} solution (106 mM NaCl, 5 mM KCl, 0.5
538 mM $CaCl_2$, 10 mM $MgCl_2$, 30 mM glucose, 10 mM HEPES) containing 1 mM Advasep-
539 7 (Biotium) to remove extracellular membrane-bound FM. Finally, cultures were washed
540 in HBS containing 20 μM CNQX and 50 μM D-AP5 for at least three times, 1 min each.
541 Next, we stimulated the microfluidic chambers using extracellular electrodes by placing a

positive and negative electrode in each well of the somatic compartment.

Electrical stimulation was provided by an AD Instrument 2 Channel Stimulus Generator (STG4002) in current mode with an asymmetric waveform (-480 µA for 1 ms and +1600 µA for 0.3 ms) for ~ 1 min at 20 hz for 600 pulses. The FM 5-95 imaging was performed as described previously [22]. Z-stacks (31 slices) were captured every 15s during the baseline (1 min), stimulation (1 min), and after stimulation (2 min) periods. This stimulation pattern was optimized for efficient FM unloading within these microfluidic chambers and the frequency is greater than typically used in open well dishes. At least 3 baseline images were acquired before electrical stimulation. Sum projected confocal z-stack were converted to 8-bit images and registered using TurboReg, an image J plugin. We background subtracted the image stack using the image 3 min after stimulation. The image stacks thresholded to a pixel value of 15. FM puncta between 2 to 50 (pixels^2) were analyzed. We measured the intensity of each punctum in the whole field or specifically on GFP labeled neuron (**fig. 3a-c**) throughout all time-series (registered stack obtained by TurboReg, imageJ plugin). To analyze the unloading kinetics of FM puncta on GFP labeled neuron, we first thresholded the GFP image and then created an outline enclosing all the GFP labeled regions including spines. The outlined ROI was superimposed on the FM labeled image and the intensity of each punctum in the selected ROI (GFP outline) was measured throughout all time series. We normalized fluorescent intensity of each puncta to the frame before stimulation. Puncta with >5% unloading after 1 min were used in the analysis as unloaded puncta. Time constants were estimated by curve fitting unloading kinetics to a single exponential decay function [22]. Curve fitting was done in MATLAB. Number of FM puncta that unload >5%

after 60s were classified as responsive using image stacks that were not background subtracted; pucnta that did not meet this criteria were classified as unresponsive.

In activity and transcription blocking experiments, the FM 5-95 unloading experiment was performed as mentioned above at 48 h post-axotomy. The intensity measurements of each punctum in the whole field and subsequent analysis of FM unloading kinetics was peformed as mentioned above.

Drug treatments. Local activity blockade solution (ABS), which includes low-Ca^{2+}, high-Mg^{2+}, and TTX (0.5 mM $CaCl_2$, 10 mM $MgCl_2$, 1 μM TTX) was applied only to axonal compartment for 1 h during axotomy. ABS solution prevents influx of sodium and reduces calcium influx. 5,6-dichloro-1-β-D-ribofuranosyl-1H-benzimidazole (DRB; Sigma-Aldrich) was suspended in DMSO and applied to the somal compartment at a final concentration of 80 μM for 1 h during axotomy. Tetrodotoxin citrate (TTX; Tocris Bioscience) was suspended in HBS and applied to the somal compartment at a final concentration of 1 μM for 1 h during axotomy. Exogenous netrin-1 was applied to the somal compartment after 1 $^1/_2$ day of axotomy, when spine changes are predominantly noticed, at a final concentration of 625ng/ml for 8-10 h. For DCC function blocking experiment, anti-DCC and isotype control (IgG) was applied to the somal compartment of uninjured cell at a final concentration of 1μg/ml for 24 h.

Microscopy. FM and fixed imaging was performed using CSU-X1 spinning disk confocal imaging unit configured for an Olympus IX81 microscope (Andor Revolution XD). Live imaging of neurons for spine analysis was captured using Zeiss LSM 780 (63x 1.4 NA or 40x 1.4 NA oil immersion objective) microscope located in UNC

588 Neuroscience Imaging core.

589

590 *Whole-Cell Electrophysiology.* For whole-cell recordings, neurons were visually
591 identified with infrared differential interference contrast optics. Cells were recorded in
592 voltage-clamp configuration with a patch clamp amplifier (Multiclamp 700A), and data
593 were acquired and analyzed using pCLAMP 10 software (Molecular Devices). Patch
594 pipettes were pulled from thick-walled borosilicate glass with open tip resistances of 2–7
595 MΩ. Series and input resistances were monitored throughout the experiments by
596 measuring the response to a −5-mV step at the beginning of each sweep. Series
597 resistance was calculated using the capacitive transient at the onset of the step and input
598 resistance was calculated from the steady-state current during the step. Recordings were
599 sampled at 10 kHz and bessel filtered at 2 kHz. No series resistance compensation was
600 applied.

601 Prior to recording, microfluidic chambers and PDMS molds were removed and
602 the glass coverslips containing cells were mounted onto a submersion chamber,
603 maintained at 32º C. Cultures were perfused at 2 mL/min with artificial cerebrospinal
604 fluid (ACSF) containing 124 mM NaCl, 3 mM KCl, 1.25 mM Na_2PO_4, 26 mM $NaHCO_3$,
605 1 mM $MgCl_2$, 2 mM $CaCl_2$ and 20 mM d-(+)-glucose, saturated with 95% O_2, 5% CO_2.
606 To determine if recorded neurons' axons entered the microfluidic chamber, 0.035 mM
607 Alexa-594 was included in all internal solutions to allow for post-hoc visualization of
608 neuronal morphology.

609 Events with a rapid rise time and exponential decay were identified as mEPSCs or
610 mIPSCs respectively using an automatic detection template in pCLAMP 10, based on

611 previously published methods[55]. mEPSC events were post-hoc filtered to only include
612 events with a peak amplitude ≥5 pA and a ≤3 ms 10-90% rise time. Mean mEPSC
613 parameters were quantified from a 10 min recording period and mIPSC parameters were
614 sampled from a 5 min recording period. Neurons were excluded from analysis if R_{series}
615 was >25 MΩ during anytime during the recording.
616
617 *mEPSCs Recordings.* mEPSC recordings were performed similar to previously
618 described[56]. AMPAR-mediated mEPSCs were isolated by voltage-clamping neurons at -
619 70 mV and by supplementing the ACSF with TTX citrate (1 μM, Abcam), the GABA (A)
620 receptor antagonist picrotoxin (50 μM, Sigma-aldrich), and the NMDA receptor
621 antagonist D, L-2-amino-5 phosphonopentanoic acid (100 μM, AP5, Abcam). The
622 internal solution contained: 100 mM $CsCH_3SO_3$, 15 mM CsCl, 2.5 mM $MgCl_2$, 5 mM
623 QX-314-Cl, 5 mM tetra-Cs-BAPTA, 10 mM HEPES, 4 mM Mg-ATP, 0.3 mM Na-GTP,
624 and 0.5% (w/v) neurobiotin with pH adjusted to 7.25 with 1 M CsOH and osmolarity
625 adjusted to ~295 mOsm with sucrose.
626
627 *mIPSC recordings.* mIPSCs were isolated by supplementing the ACSF with TTX
628 citrate (1 μM), the NMDA receptor antagonist AP5 (100 μM), and the AMPA/Kainate
629 receptor antagonist 6,7-dinitroquinoxaline-2,3-dione (20 μM, DNQX, dissolved in
630 DMSO for a final concentration of 1% v/v DMSO in ACSF, Abcam). For mIPSC
631 recordings, the pipette solution contained a relatively lower chloride concentration,
632 similar to intracellular chloride concentrations that are present in more mature neurons [57].
633 This pipette solution contained, 110 mM $CsCH_3SO_3$, 2.5 mM $MgCl_2$, 5 mM QX-314-Cl,

5 mM tetra-Cs-BAPTA, 10 mM HEPES, 4 mM Mg-ATP, 0.3 mM Na-GTP, and 0.5% (w/v) neurobiotin with pH adjusted to 7.28 with 1 M CsOH and a 300 mOsm osmolarity. Following break-in, neurons were first voltage-clamped at -70 mV for at least three minutes to allow dialysis with pipette solution, after which the voltage was gradually changed to 0 mV, where it was maintained for duration of the recording.

SCI injury and in vivo electrophysiology. Nineteen adult male, Fischer-344 inbred rats (Harlan Laboratories, Indianapolis, IN) were selected for this study. A total of 14 rats received a contusion injury in the thoracic cord at level T9–T10, whereas 5 rats were randomly selected as uninjured controls. After a minimum of 4 weeks following SCI, intracortical microstimulation (ICMS) and single-unit recording techniques were used in the hindlimb motor area (HLA) to determine movements evoked by ICMS and spike rates. The protocol was approved by the University of Kansas Medical Center Institutional Animal Care and Use Committee.

Spinal cord surgeries were performed under ketamine hydrochloride (80 mg/kg)/xylazine (7 mg/kg) anesthesia and aseptic conditions. Each of the SCI rats underwent a T9–T10 laminectomy and contusion injury using an Infinite Horizon spinal cord impactor (Precision Systems and Instrumentation, LLC, Fairfax Station, VA) with a 200 Kdyn impact. At the conclusion of surgery, 0.25% bupivacaine hydrochloride was applied locally to the incision site. Buprenex (0.01mg/kg, SC) was injected immediately after surgery and 1 day later. On the first week after surgery, the rats received daily injections of 30,000U penicillin in 5mL saline. Bladders were expressed twice daily until the animals recovered urinary reflexes.

Post-SCI surgical and neurophysiological procedures were conducted under aseptic conditions 4 to 18 weeks post-SCI. At the time of these procedures, ages ranged from 4.5 to 7.5 months. After an initial, stable anesthetic state was reached using isoflurane anesthesia, isoflurane was withdrawn and the first dose of ketamine hydrochloride (100 mg/kg)/xylazine (5 mg/kg) was administered. The rats were placed in a Kopf small-animal stereotaxic instrument and a craniectomy was performed over the motor cortex. The dura was incised and the opening filled with warm, medical grade, sterile silicone oil. Core temperature was maintained within normal physiological limits using a feedback-controlled heating pad during the entire procedure. A stable anesthetic level was assessed by monitoring the respiratory and heart rate, and reflexes to noxious stimuli.

In each rat, neuronal recordings were begun at ~3 h after initiation of the procedure. Neuronal action potentials (single-units or spikes) were recorded with a single-shank, 16-channel Michigan-style linear microelectrode probe (Neuronexus, Ann Arbor, MI). A total of 15 channels were active in each procedure. The tip of the probe was lowered to a depth of 1720 μm below the cortical surface, allowing accurate determination of depth for each recording site. Because no hindlimb responses were evoked using ICMS in SCI rats, the location of HLA in SCI rats was determined by the stereotaxic coordinates derived in normal rats in a previous study (centered at 2mm posterior and 2.64mm lateral to bregma). At each cortical location, electrical activity was collected and digitized for 5 min from each of the 15 active sites using neurophysiological recording and analysis equipment (Tucker Davis Technologies, Alachua, FL). Neural spikes were discriminated using principle component analysis.

680 Sample waveforms (1.3 msec in duration) were collected that passed 5.5 X SD below
681 root mean square (RMS). After each experiment, the probe was cleaned with Opti-Free
682 solution (Alcon Laboratories, Fort Worth, TX), followed by ethanol and then rinsed
683 thoroughly in distilled water. The electrode impedance of each site remained at 0.9MΩ
684 for each experiment. At the end of the recording session, rats were humanely euthanized
685 with an overdose of sodium pentobarbital.
686
687 *Statistics.* Graphpad prism 6 statistical program was used. For calculating
688 significance on spine density in live imaging data, paired two-tailed t-test was performed.
689 Unpaired two-tailed t-test was performed when comparing two independent groups. For
690 FM unloading experiments and for comparing multiple groups, Two-way ANOVA and
691 One-way ANOVA were used respectively followed by Bonferroni post-hoc test. For
692 patch-clamp electrophysiology experiments, unpaired two-tailed t-tests or unpaired two-
693 tailed t-tests with Welch's correction were performed to compare two groups. For *in vivo*
694 experiments, hypotheses regarding spike firing rates were tested independently in each
695 cortical layer (Va, Vb and VI) using a two-tailed t-test, (alpha = 0.05).
696
697

698 References:

699 1. Nudo, R.J. *Front Hum Neurosci* **7**, 887 (2013).

700 2. Takechi, U., *et al. Clin Neurophysiol* **125**, 2055-2069 (2014).

701 3. Nudo, R.J. & Milliken, G.W. *J Neurophysiol* **75**, 2144-2149 (1996).

702 4. Oudega, M. & Perez, M.A. *J Physiol* **590**, 3647-3663 (2012).

703 5. Frost, S.B., *et al. J Neurophysiol* **89**, 3205-3214 (2003).

704 6. Rishal, I. & Fainzilber, M. *Nat Rev Neurosci* **15**, 32-42 (2014).

705 7. Urban, E.T., 3rd, *et al. Molecular and cellular biochemistry* **369**, 267-286 (2012).

706 8. Kim, B.G., *et al. Exp Neurol* **198**, 401-415 (2006).

707 9. Jacobs, K.M. & Donoghue, J.P. *Science* **251**, 944-947 (1991).

708 10. Ding, M.C., *et al. J Neurosci* **31**, 14085-14094 (2011).

709 11. Nakatomi, H., *et al. Cell* **110**, 429-441 (2002).

710 12. Will, B., *et al. Progress in Neurobiology* **72**, 167-182 (2004).

711 13. Taylor, A.M., *et al. J Neurosci* **29**, 4697-4707 (2009).

712 14. Taylor, A.M., *et al. Nat Methods* **2**, 599-605 (2005).

713 15. Banker, G.A. & Cowan, W.M. *Brain Res* **126**, 397-342 (1977).

714 16. Benson, D.L., *et al. J Neurocytol* **23**, 279-295 (1994).

715 17. Greer, J.E., *et al. J Neurosci* **32**, 6682-6687 (2012).

716 18. Ikeda, S. & Nakagawa, S. *Brain Res* **792**, 164-167 (1998).

717 19. McIlwain, D.L. & Hoke, V.B. *BMC Neurosci* **6**, 19 (2005).

718 20. Ghosh, A., *et al. Cereb Cortex* **22**, 1309-1317 (2012).

719 21. Gao, X., *et al. PLoS One* **6**, e24566 (2011).

720 22. Taylor, A.M., *et al. J Neurosci* **33**, 5584-5589 (2013).

721 23. Zakharenko, S.S., *et al. Nat Neurosci* **4**, 711-717 (2001).

722 24. Taylor, A.M., *et al. Neuron* **66**, 57-68 (2010).

723 25. Frost, S.B., *et al. J Neurotrauma* **32**, 1666-1673 (2015).

724 26. Lewicki, M.S. *Network* **9**, R53-78 (1998).

725 27. Nudo, R.J., *et al. The Journal of Comparative Neurology* **358**, 181-205 (1995).

726 28. Barron, K.D., *et al. J Neuropathol Exp Neurol* **47**, 62-74 (1988).

727 29. Li, P. & Zhuo, M. *Nature* **393**, 695-698 (1998).

728 30. Bekkers, J.M. *J Neurosci* **25**, 4031-4039 (2005).

729 31. Chen, J.L., *et al. Neuron* **74**, 361-373 (2012).

730 32. Markram, H., *et al. Nat Rev Neurosci* **5**, 793-807 (2004).

731 33. Chiu, C.Q., *et al. Science* **340**, 759-762 (2013).

732 34. Higley, M.J. *Nat Rev Neurosci* **15**, 567-572 (2014).

733 35. Horn, K.E., *et al. Cell Rep* **3**, 173-185 (2013).

734 36. Goldman, J.S., *et al. J Neurosci* **33**, 17278-17289 (2013).

735 37. Shadiack, A.M., *et al. J Neurosci* **21**, 363-371 (2001).

736 38. Xu, K., *et al. Science* **344**, 1275-1279 (2014).

737 39. Manitt, C., *et al. J Neurosci* **29**, 11065-11077 (2009).

738 40. Wong, Y.C. & Holzbaur, E.L. *J Neurosci* **34**, 1293-1305 (2014).

739 41. Branco, T., *et al. Neuron* **59**, 475-485 (2008).

740 42. Stavoe, A.K. & Colon-Ramos, D.A. *The Journal of Cell Biology* **197**, 75-88

741 (2012).

742 43. Colon-Ramos, D.A., *et al. Science* **318**, 103-106 (2007).

743 44. Manitt, C., *et al. J Neurosci Res* **84**, 1808-1820 (2006).

744 45. Ahn, K.J., *et al. Neurosci Lett* **419**, 43-48 (2007).

745 46. Lu, H., *et al. Front Med* **5**, 86-93 (2011).

746 47. Han, X., *et al. Mol Neurobiol* (2016).

747 48. Sun, H., *et al. Neurobiol Dis* **44**, 73-83 (2011).

748 49. Blue, M.E. & Parnavelas, J.G. *J Neurocytol* **12**, 697-712 (1983).

749 50. Bolshakov, V.Y. & Siegelbaum, S.A. *Science* **269**, 1730-1734 (1995).

750 51. Wickersham, I.R., *et al. Neuron* **53**, 639-647 (2007).

751 52. Fu, M.M. & Holzbaur, E.L. *Autophagy* **10**, 2079-2081 (2014).

752 53. Nagendran, T. & Hardy, L.R. *Neuroscience* **199**, 548-562 (2011).

753 54. Rodriguez, A., *et al. PLoS One* **3**, e1997 (2008).

754 55. Clements, J.D. & Bekkers, J.M. *Biophys J* **73**, 220-229 (1997).

755 56. Larsen, R.S., *et al. Neuron* **83**, 879-893 (2014).

756 57. Yamada, J., *et al. J Physiol* **557**, 829-841 (2004).

757

758

759 **Acknowledgements:** We thank Stephanie Gupton for netrin-1, Kelly Carstens for

760 preliminary gene expression work, and Cassie Meeker for technical support. We thank

761 Richard Segal (MUSC), Julius Dewald (RIC) and Taylor lab members for their advice

762 and discussions. **Funding:** A.M.T. acknowledges support from the Eunice Kennedy

763 Shriver NICHD (K12 HD073945), NIMH (R42 MH097377), and an Alfred P. Sloan

764 Research Fellowship. We acknowledge funding from a neuroscience center grant P30

765 NS045892. R.S.L was supported by NRSA predoctoral fellowship F31 MH091817 and

766 the UNC Department of Cell Biology and Physiology's Dr. Susan Fellner fellowship.

767 R.L.B. was supported in part by a grant from the National Institute of General Medical
768 Sciences under award 5T32 GM007092. **Author contributions:** T.N. designed and
769 performed experiments and wrote the manuscript. R.S.L. designed and performed
770 electrophysiology experiments. R.L.B. designed and performed experiments.. S.B.F.
771 performed experiments. B.D.P. designed experiments. R.J.N. designed and performed
772 experiments. A.M.T. designed experiments and wrote the manuscript. **Competing**
773 **financial interests:** Yes there is potential competing interest. A.M.T. is an inventor of
774 the microfluidic chambers (US 7419822 B2) and has financial interest in Xona
775 Microfluidics, LLC. T.N., R.L.B., R.S.L., R.J.N. and B.D.P. declare no competing
776 financial interests.
777

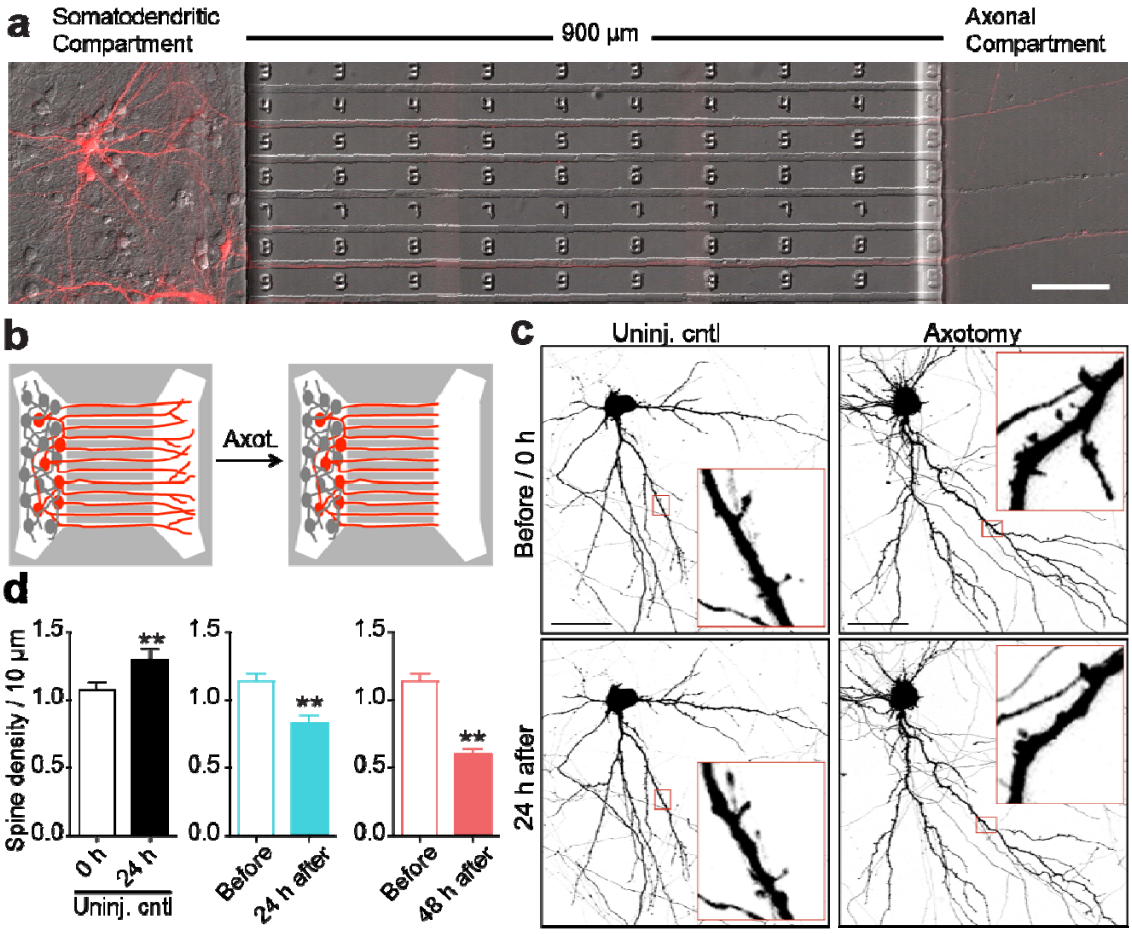

Figure 1: Distal axotomy of pyramidal neurons within microfluidic chambers induced dendritic spine loss on axotomized neurons. (**a**) 14 DIV rat hippocampal neurons cultured within a microfluidic chamber. Pyramidal neurons were retrogradely labeled using a G-deleted rabies mCherry virus added exclusively to the axonal compartment. (**b**) Cartoon illustration of *in vitro* axotomy (Axot.) within microfluidic chambers which axotomized a subset of neurons (red) that extended their axons through the microgrooves. Axons of uninjured neurons (grey) were housed within the somatodendritic compartment. (**c**) Representative images of neurons and dendritic segments, retrogradely labeled with G-deleted rabies-mCherry virus (inverted), from repeated live imaging of uninjured control (Uninj. cntl) and axotomized neurons at 0 h or

789 before axotomy and 24 h after. Image and inset scale bars, 50 and 5 μm, respectively.

790 Paired two-tailed t-test, **$p \leq 0.001$; 20 primary dendritic process were analyzed from 5

791 individual neurons over two-independent experiments. Error bars, SEM.

792

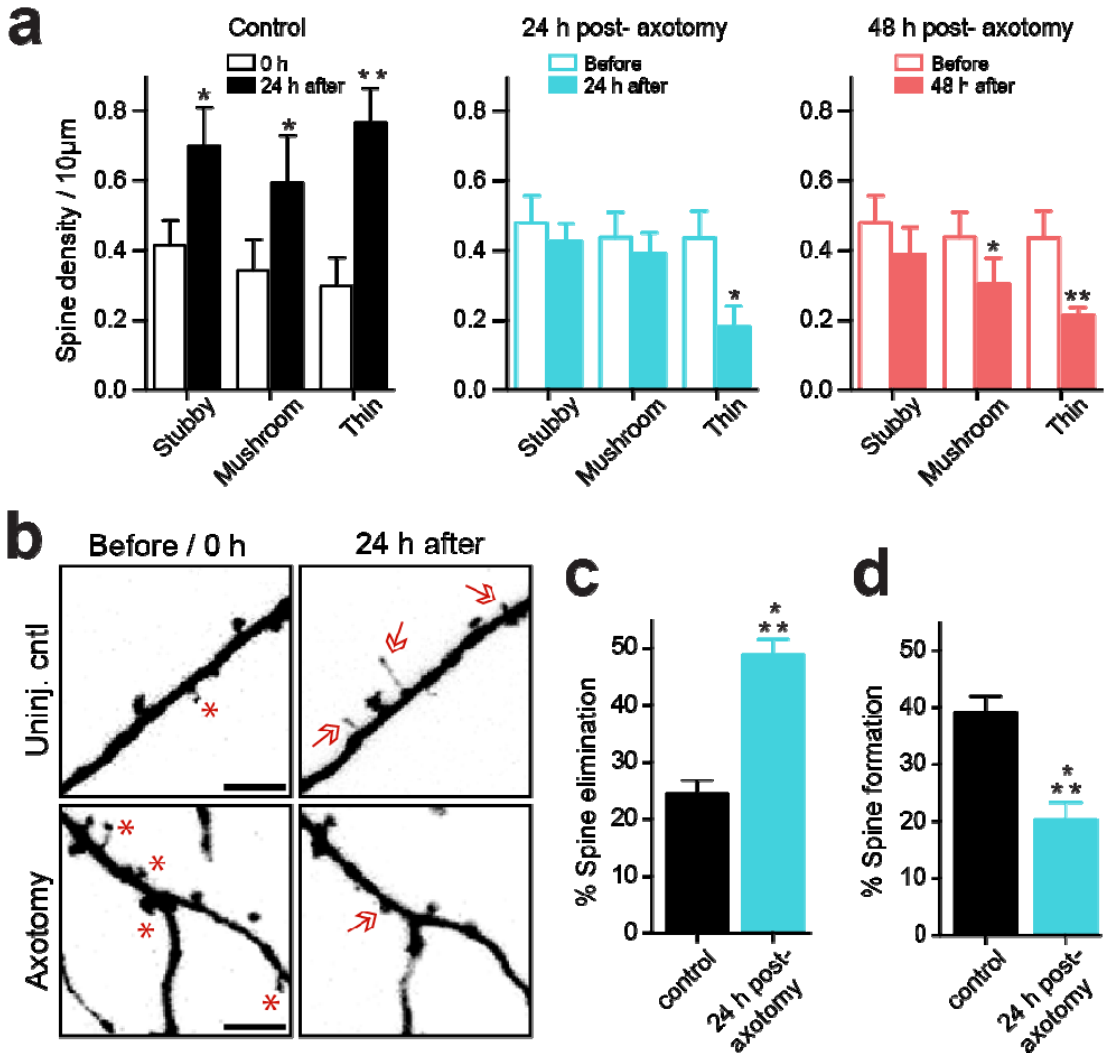

Figure 2: Axotomy increased the elimination of dendritic spines, reduced new spine formation, and led to the preferential absence of thin spines. (a) Distribution of spine categories in live uninjured controls (before: black open bars; 24 h after: black solid bars), 24 h post-axotomy (before; blue open bars; 24 h after: blue solid bars) and 48 h post-axotomy (before; red open bars; 48 h after: red solid bars). Two-way ANOVA, Bonferroni post hoc test, * $p < 0.05$, ** $p < 0.01$. (b) Representative images of dendritic segments from uninjured control and axotomized neurons at 0 h or before axotomy and 24 h after. Astericks indicate the spines eliminated overtime and arrows indicate

802 formation of new spines 24 h after axotomy. Scale bars, 5 µm. Bar graphs represent
803 percentage of spines that were eliminated (c) and newly formed (d) after 24 h in
804 uninjured controls (Uninj. cntl) and 24 h post-axotomy. Two-tailed t-test, *** $p < 0.001$.
805 (a,c, and d) These analyses represent 20 primary dendritic processes from 5 live neurons
806 per condition over two independent experiments. The same trend was observed in each
807 independent experiment. Error bars, SEM.
808

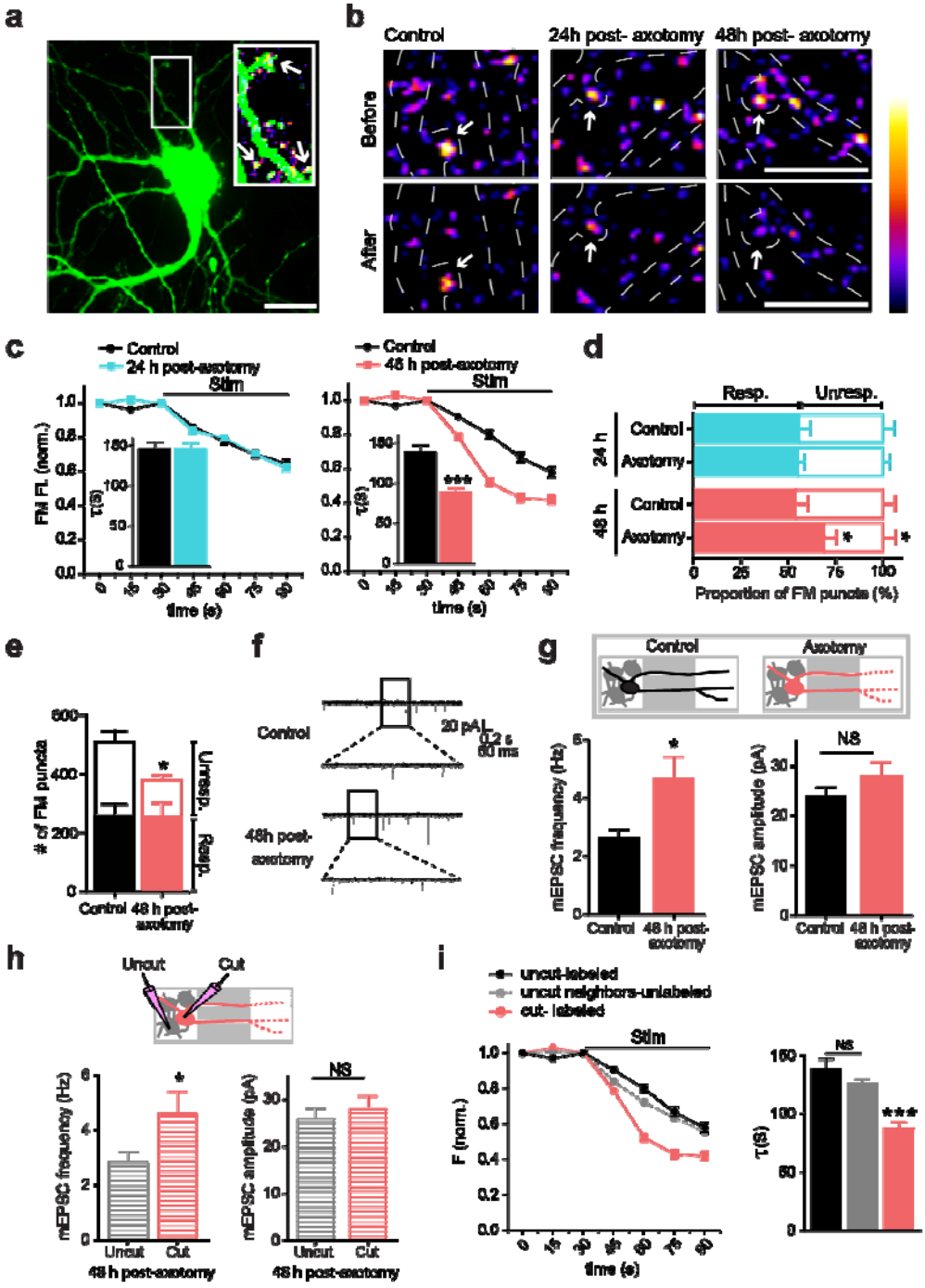

Figure 3: Distal axotomy induced a delayed trans-synaptic increase in presynaptic-excitability onto axotomized neurons.

(**a**) Representative image of a neuron retrogradely labeled with a modified eGFP rabies virus within the somatodendritic compartment of a microfluidic chamber. Inset shows an

814 enlarged region demonstrating colocalization of FM puncta with eGFP-labeled dendrites
815 and dendritic spines (arrows). FM puncta were visualized using the ImageJ 'fire' color
816 look up table shown in *(b)*. Scale bar, 20 µm. (b) Representative images show FM puncta
817 before and after field stimulation. Boundaries of eGFP labeled dendrites and spines are
818 outlined as white dashed lines. Arrows in the before and after stimulation images indicate
819 destaining of FM labeled puncta at dendritic spines. Scale bars, 10 µm. (**c**) FM unloading
820 curves from FM puncta colocalized onto GFP labeled neurons at 24 h post-axotomy
821 (control, n=124 puncta combined from 3 chambers; axotomy, n=156 puncta combined
822 from 3 chambers over two independent experiments) and 48 h post-axotomy (control,
823 n=160 puncta combined from 3 chambers; axotomy, n=220 puncta combined from 3
824 chambers over 2 independent experiments). Two-way ANOVA, Bonferroni post hoc test,
825 ***$p \leq 0.001$. Insert: decay time constant (τ) of FM puncta at 24 h and 48 h post-
826 axotomy. Unpaired two-tailed t-test, ***$p < 0.001$. Data shown represent 2 independent
827 experiments. (**d**) Percent responsive FM puncta and unresponsive FM puncta at 24 h
828 (control, n=1,431; axotomy, n=1,602; data shown are from 2 independent experiments
829 which includes a total of 4 chambers for each condition) and 48 h post-axotomy (control,
830 n=3,452; axotomy, n=2,793; data shown is from 3 independent experiments to yield a
831 combined 7 chambers for each condition). Asterisks indicate that the percentage of
832 responsive and unresponsive puncta at 48 h post-axotomy is significantly different from
833 control. Unpaired two-tailed t-test, *$p < 0.05$. (**e**) Total number of responsive and
834 unresponsive FM puncta at 48 h post-axotomy (Resp: control, n=1,536; axotomy,
835 n=1,522; Unresp: control, n=1,504; axotomy, n=742; data shown represents 3
836 independent experiments which combined included 6 chambers for each condition)

837 Unpaired two-tailed t-test, *p< 0.05. (**f**) Representative traces of mEPSC recordings 48 h
838 post-axotomy. (**g**) Quantification of mEPSC frequency and amplitude at 48 h post-
839 axotomy (control, n=17 neurons; axotomy, n=20 neurons). Data shown were combined
840 from 4 independent experiments. Neurons from axotomized microfluidic devices had an
841 increased mEPSC frequency compared to uninjured control devices (mEPSC frequency:
842 unpaired two-tailed t-test with Welch's correction, *p < 0.05; mEPSC amplitude:
843 unpaired two-tailed t-test, p = 0.2). Insert: Cartoon depicts recordings from either control
844 neurons within uninjured chambers (*g*; black) or directly injured neurons within
845 chambers subjected to axotomy (red). (**h**) Analysis of mEPSC frequency and amplitude
846 from axotomy devices previously shown in (g) comparing neurons with axons that
847 extended into the axonal compartment and were cut (cut, n=10 neurons), to neurons that
848 did not extend axons into the compartment and were not cut (uncut, n=10 neurons).
849 Axotomized neurons had increased mEPSC frequency compared to their uninjured
850 neighbors from the same device (mEPSC frequency: unpaired two-tailed t-test with
851 Welch's correction, *p < 0.05; mEPSC amplitude: unpaired two-tailed t-test, p = 0.52).
852 Insert: Cartoon depicts recordings from either a directly injured neuron (*h*; red) or its
853 neighboring uninjured neuron (grey). (**i**) FM unloading curves of neighboring uninjured
854 neurons (uncut neighbors, n=767 puncta combined from 4 chambers) within axotomized
855 chambers, identified by lack of eGFP labeling, were compared with uninjured control
856 neurons (uncut) and axotomized neurons labeled with eGFP rabies virus at 48 h post-
857 axotomy. Two-way ANOVA, Bonferroni post hoc test ***p <0.001. Decay time constant
858 (τ) of FM puncta at 48 h post-axotomy. One-way ANOVA, Bonferroni post hoc test ***p
859 <0.001. Data shown represent 2 independent experiments. Error bars, SEM.

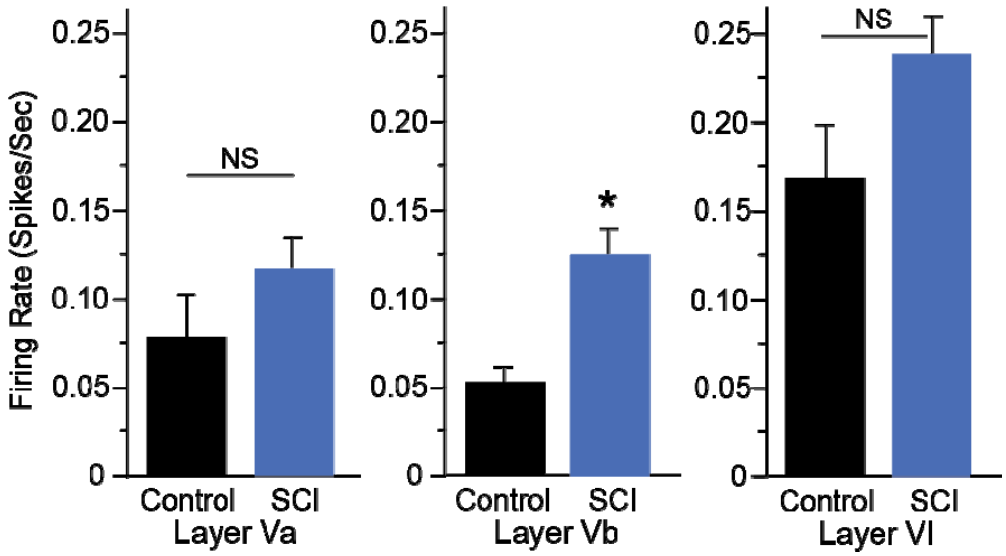

860 **Figure 4: Spinal cord injury results in increased spontaneous single-unit firing rate**
861 **in layer Vb of hindlimb cortex 4-18 weeks following injury.**

862 Mean spontaneous firing rates of isolated single-units in layers Va, Vb and VI of the
863 hindlimb motor cortex in control rats (n = 5) and rats with a spinal cord contusion at T9-
864 10 (n = 14). Laminar estimates are based on the depths of electrode sites on a single-
865 shank multi-electrode array relative to the cortical surface [25]. In each rat, single-unit
866 (spike) activity was sampled from 4 to 6 locations within the neurophysiologically-
867 identified hindlimb motor cortex. Data represent the mean firing rates of 1,744 isolated
868 units in Layers Va (control, n=124; SCI, n=312), Vb (control, n=155; SCI, n=390), and
869 VI (control, n=217; SCI, n=546). Asterisk indicates that the firing rate of single-units in
870 layer Vb of spinal cord injured rats is significantly higher compared to firing rates in
871 control rats. Two-tailed t-test, t=3.99, *p<0.0001.
872

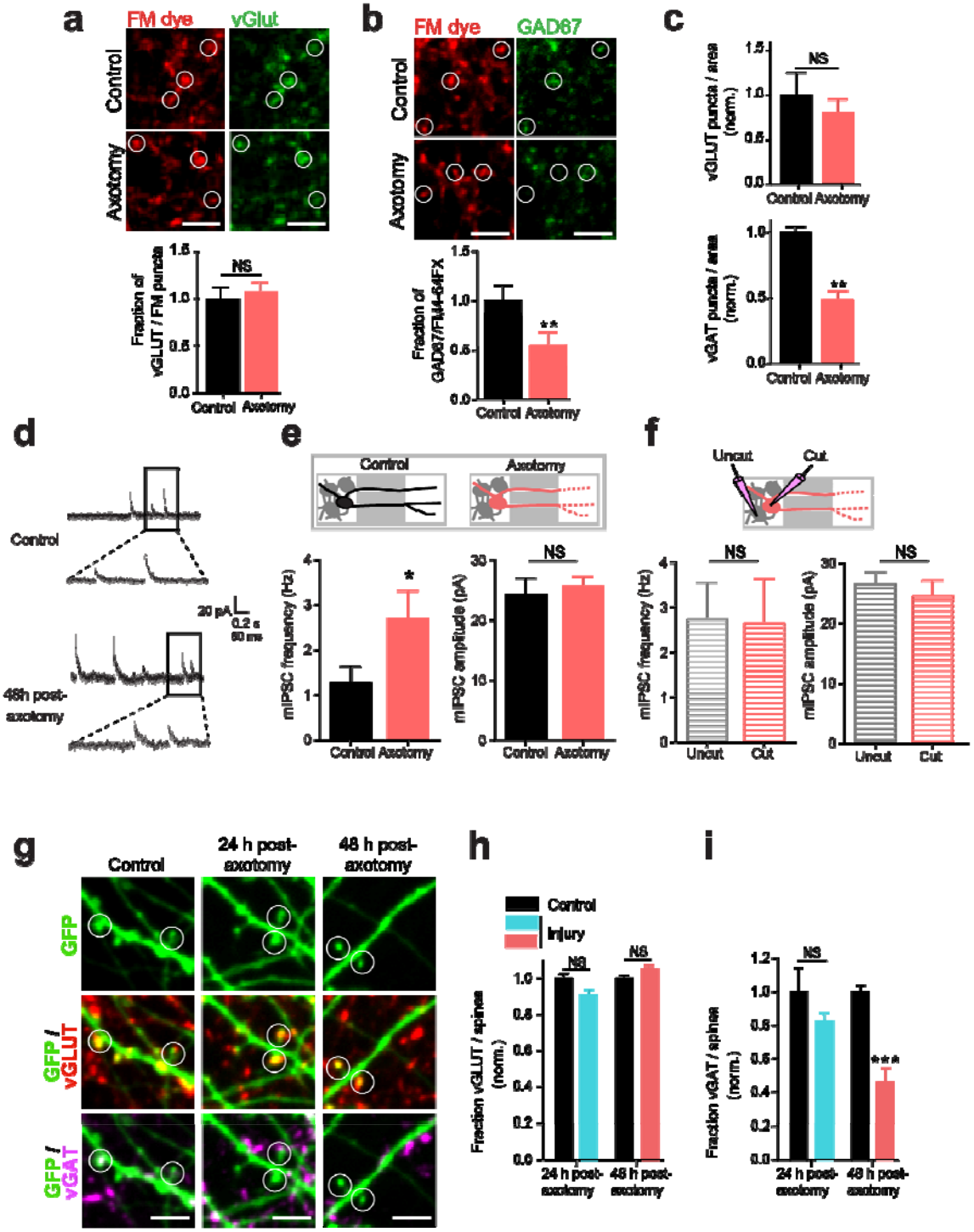

Figure 5: Distal axotomy induces culture-wide loss of inhibitory terminals, increased spontaneous GABAergic neurotransmission, and selective loss of inhibited spine synapses onto injured neurons.

(**a**) Representative images showing fixable FM4-64FX puncta (red) and vGlut (green) labeling. White open circles highlight vGlut expression in FM labeled terminals. Scale bars, 10 µm. vGlut1 positive FM puncta at 48 h post-axotomy normalized to control. 10 individual fields were analyzed per condition. (**b**) Images showing fixable FM4-64FX puncta (red) and GAD67 (green) labeling. White open circles highlight GAD67 expression levels in FM labeled terminals. Scale bars, 10 µm. Fraction of GAD67-positive FM puncta at 48 h post-axotomy normalized to control. 10 individual fields were analyzed per condition. (**c**) Density of vGLUT1 and vGAT puncta in an area following 48 h post-axotomy, normalized to controls. N= 4 individual neurons were analyzed per condition. (a-c) Unpaired two-tailed t-test, $^{**}p < 0.01$. (**d**) Representative traces of mIPSC recordings 48 h post-axotomy. (**e**) Quantification of mIPSC frequency and amplitude at 48 h post-axotomy (control, n=9 neurons; axotomy, n=17 neurons). Neurons from axotomized microfluidic devices have an increased mIPSC frequency compared to uninjured control devices (mIPSC frequency: unpaired two-tailed t-test with Welch's correction, $p = 0.05$; mIPSC amplitude: unpaired two-tailed t-test, $p = 0.62$). (**f**) Analysis of mIPSC frequency and amplitude from axotomy devices previously shown in (e) comparing neurons with axons that extended into the axonal compartment and were cut (cut, n=8 neurons), to neurons that did not extend axons into the compartment and were not cut (uncut, n=9 neurons). Axotomized neurons and their their uninjured neighbors from the same device have a similar mean mIPSC frequency and amplitude, suggesting axotomy increases spontaneous GABAergic neurotransmission both at injured and uninjured neighboring neurons (mIPSC frequency: unpaired two-tailed t-test, $p = 0.94$; mIPSC amplitude: unpaired two-tailed t-test, $p = 0.51$). (**g**) Representative dendritic

900 segments (retrogradely labeled with GFP) showing spines that are labeled with either
901 vGLUT (red) or vGAT (purple) antibodies. White open circles highlight dendritic spines
902 with vGLUT and/or vGAT synapses. (**h**) Fraction of vGlut positive dendritic spines at 24
903 h and 48 h post-axotomy normalized to respective controls. (**i**) Fraction of vGAT positive
904 dendritic spines at 24 h and 48 h post-axotomy normalized to respective controls. 8
905 individual fields were analyzed per condition from two independent experiments. The
906 same trend was observed in each experiment. Scale bars, 5 µm. Two-tailed t-test, ***$p \leq$
907 0.001. Error bars, SEM.
908
909

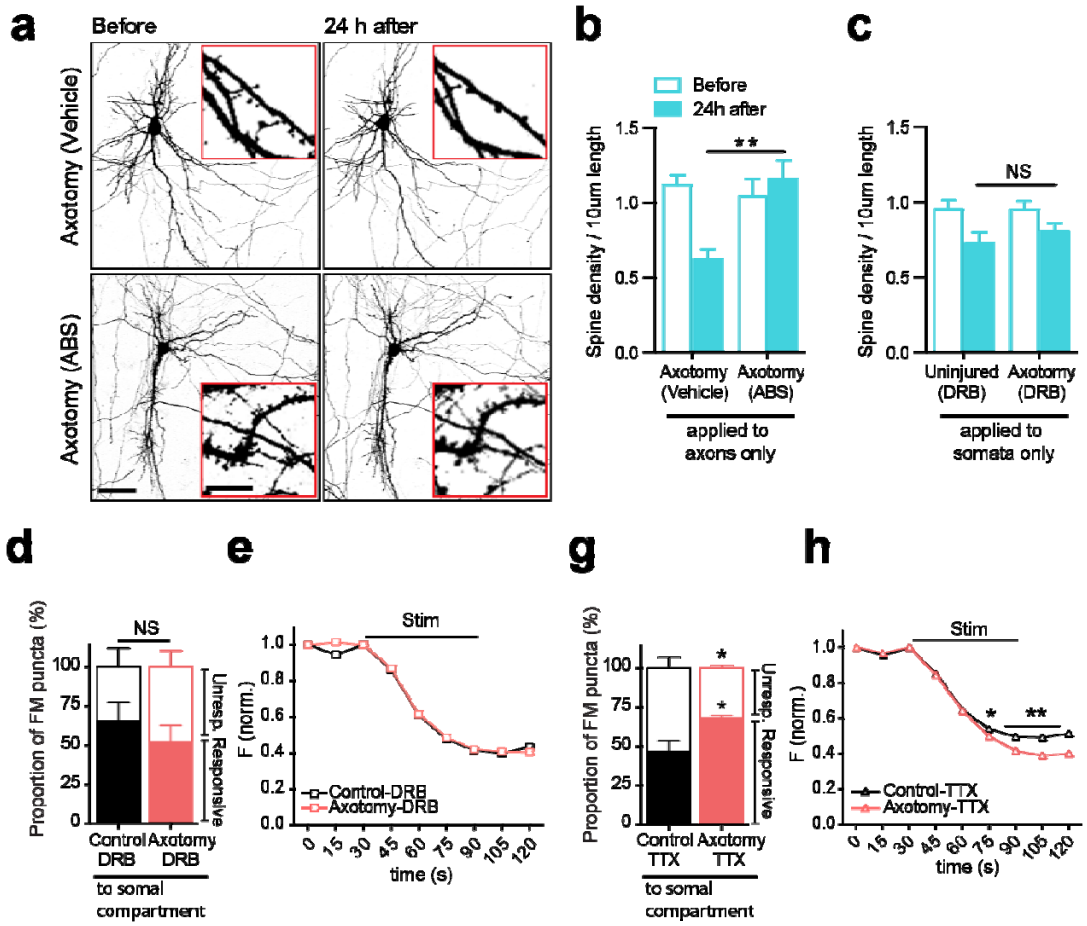

Figure 6: Injury-induced synaptic changes are triggered by retrograde propogation of injury signal from axon to soma and gene transcription.

(**a**) Representative images of neurons retrograde labeled with modified eGFP rabies virus (inverted grayscale) before and 24 h after axotomy in the presence of vehicle or local activity blockade solution (ABS) applied to axonal compartment for 1 h during axotomy. Axotomy and imaging were performed within microfluidic chambers. Inset shows zoomed in dendritic region. (**b**) Quantification of spine density results described in (a). (**c**) Quantification of spine density changes following application of transcription blocker (DRB) to the somatodendritic compartment for 1 h prior to and during injury. (**c, d)** Analyzed 20 primary dendritic process from 4 live neurons per condition over two

independent experiments. Repeated measure two-way ANOVA, Bonferroni post hoc test, **p<0.001. (**d**) Percent of unloaded FM puncta (responsive) and unresponsive puncta at 48 h post-axotomy. Approximately 300 puncta were analyzed per chamber; 4 individual chambers were analyzed per condition over two independent experiments. Unpaired two-tailed t-test. (**e**) FM5-95 unloading following application of DRB. Approximately 200 puncta were analyzed per chamber; 4 individual chambers were analyzed per condition over two independent experiments. (**f**) Percent of unloaded FM puncta (responsive) and unresponsive puncta at 48 h post-axotomy following application of action potential blocker (TTX) to the somatodendritic compartment prior to and during injury. Approximately 400 puncta were analyzed per chamber; 4 individual chambers were analyzed for each condition over two independent experiments. Asterisks indicate that the percentage of responsive and unresponsive puncta is significantly different compared to control. Unpaired two-tailed t-test, *$p < 0.05$. (**g**) FM5-95 unloading curves following application of TTX. Approximately 200 puncta were analyzed per chamber; 4 individual chambers were analyzed for each condition over two independent experiments). The same trend was observed in each pair of experiments. Two-way ANOVA, Bonferroni post hoc test, *$p < 0.05$, **$p < 0.01$. Error bars, SEM.

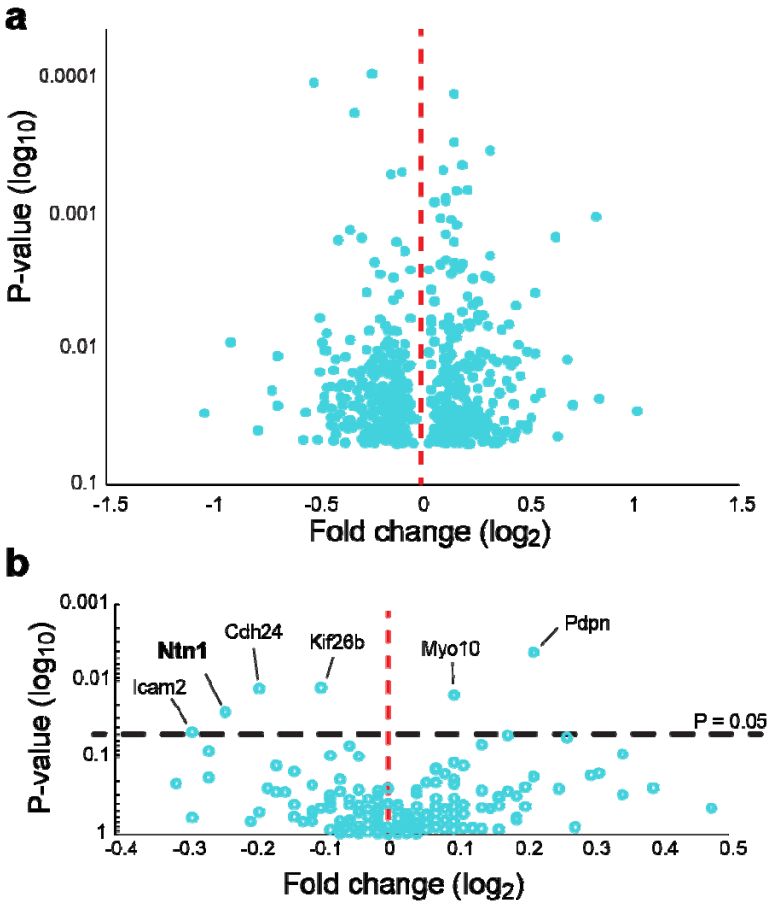

939

940 **Figure 7: Cell-cell adhesion transcripts were differentially expressed within the**

941 **somatodendritic compartment 24 h post-axotomy.**

942 Microarray analysis was performed on somatodendritic samples of controls and 24 h

943 post-axotomy cultures. (A) Volcano plot showing differentially expressed RNAs that are

944 significantly changed at 24 h post-axotomy (p-value < 0.05; n = 3 individual chambers

945 each condition; **Table supplement 2**). (B) Volcano plot showing differential expression

946 of transcripts from Gene Ontology biological process category "cell-cell adhesion". Only

947 6 transcripts are significantly changed in this category (**Table supplement 3**). One-way

948 ANOVA, p-value < 0.05 represents the transcripts that are consistently changed in each

949 of the three microarray datasets.

950

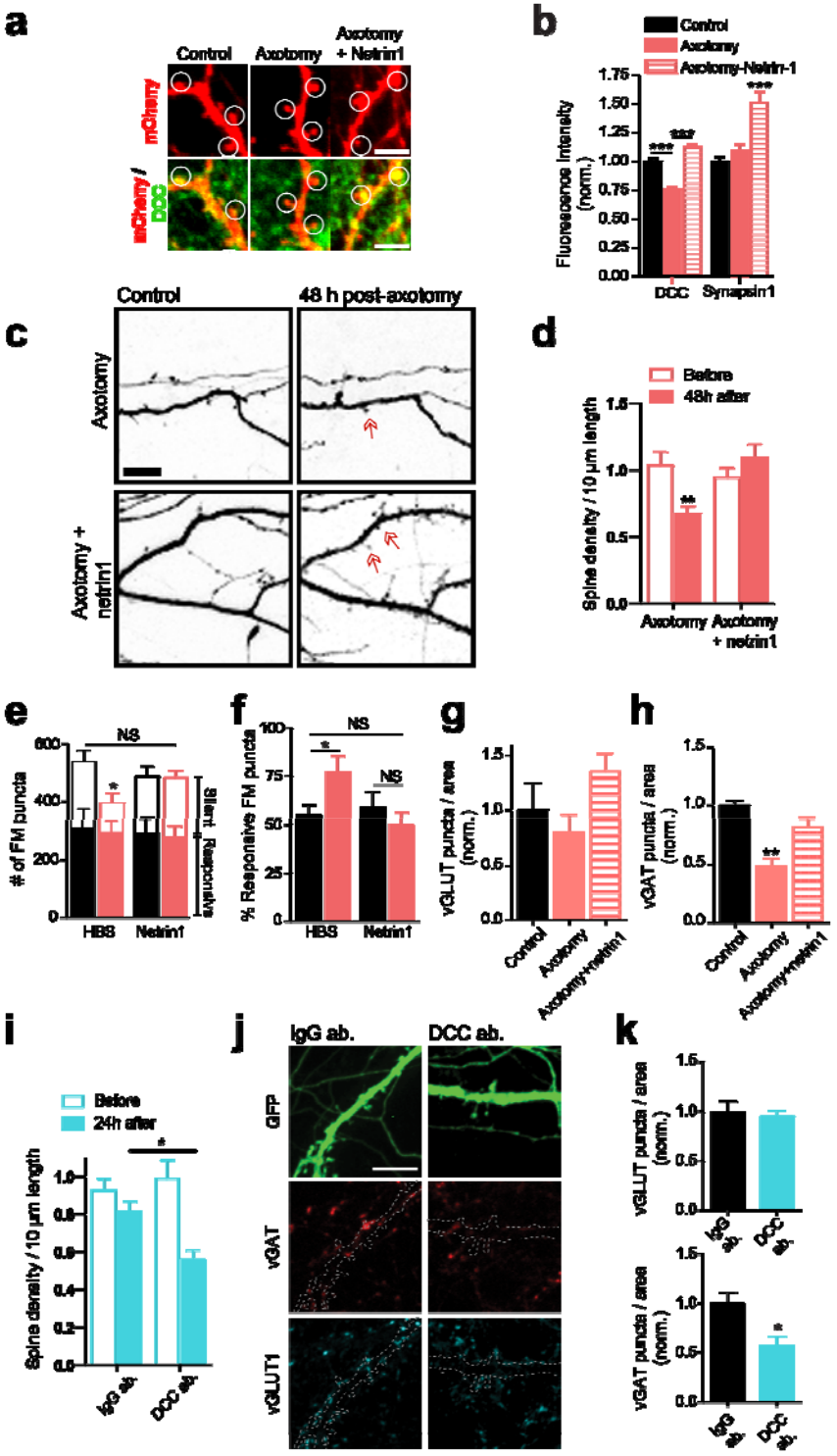

951

952 **Figure 8: Exogenous netrin-1 rescues post and presynaptic changes following distal**

953 **axotomy.**

954 (**a**) Representative images of fixed dendritic segments, retrogradely labeled with G-
955 deleted rabies-mCherry virus and immunostained with DCC antibody following
956 exogenous netrin-1 treatment. Regions of interest (ROI's; white circles) show synaptic
957 DCC levels at 48 h post-axotomy. Scale bar, 10 μm. (**b**) Quantification of DCC
958 fluorescence intensity at 48 h post-axotomy and in response to exogenous application of
959 netrin-1 (control, n=185 ROIs; axotomy, n=165 ROIs; axotomy + netrin-1, n=100 ROIs).
960 At least 4 individual chambers were analyzed per condition from two independent
961 experiments. The same trend was observed in each independent experiment. Two-way
962 ANOVA, Bonferroni post hoc test, ***$p < 0.001$. (**c**) Representative images of dendritic
963 segments from before axotomy and 48 h after of an axotomized neuron treated with either
964 vehicle (HBS) or netrin-1. Arrows indicate formation of new spines over 48 h period
965 following axotomy. Scale bars, 10 μm. (**d**) Change in spine density at 48 h post-axotomy
966 and in response to exogenous application of netrin1. Repeated measure two-way
967 ANOVA, Bonferroni post hoc test, ** $p < 0.01$. Analyzed 20 primary dendrites from
968 5 live neurons per condition over two independent experiments. (**e**) Average number of
969 responsive and unresponsive FM puncta per field in response to exogenous application of
970 netrin-1 48 h post-axotomy. Approximately 400 puncta were analyzed per chamber from
971 7 individual chambers for each condition. Data shown was from two independent
972 experiments and a similar trend was observed in each these experiment. One-way
973 ANOVA, Bonferroni post hoc test, *$p < 0.05$. Noticeably, injury decreased the number of
974 unresponsive FM puncta that was normalized in response to exogenous application of
975 netrin-1 48 h post-axotomy. (**f**) The percent of responsive FM puncta (unloaded puncta)
976 following exogenous application of netrin-1 48 h post-axotomy. Two-tailed t-test, *p <

977 0.05. (**g**) Density vGLUT1 and (**h**) vGAT puncta in an area following exogenous netrin-1
978 application, normalized to vehicle (HBS) controls. N= 4 individual neurons were
979 analyzed per condition. One-way ANOVA, Bonferroni post hoc test,**p < 0.01. (**i**)
980 Quantification of spine density following 24 h application of either control antibody (IgG
981 ab.) or DCC function blocking antibody (DCC ab.). Repeated measure two-way
982 ANOVA, Bonferroni post hoc test, * p < 0.05. Analyzed 20 primary dendrites from 5 live
983 neurons per condition over two independent experiments. (**j**) Representative images of
984 fixed dendritic segments, retrogradely labeled with G-deleted rabies-mCherry virus and
985 immunostained with vGLUT1 and vGAT antibody following 24 h application of either
986 control antibody (IgG ab) or DCC function blocking antibody (DCC ab). Scale bar,
987 10µm. (**k**) Density of vGLUT1 and vGAT puncta in an area following 24 h application of
988 either control antibody (IgG ab.) or DCC function blocking antibody (DCC ab.),
989 normalized to vehicle (HBS) controls. N= 9 individual field per condition. Similar trend
990 was observed in each of the two independent experiments. Unpaired two-tailed t-test, *p
991 < 0.05. Error bars, SEM.
992
993

994 **Supplemental figures and tables:**

995 **Figure supplement 1:** Distal axotomy of pyramidal neurons induces dissolution of Nissl
996 substance without affecting cell viability.

997 **Figure supplement 2:** Dendrites retract, show fewer branch points and spines 24 h post-
998 axotomy compared to uninjured controls.

999 **Figure supplement 3:** FM puncta highly colocalizes with synapsin1 immunolabeling.

1000 **Figure supplement 4:** FM unloading curves from somatodendritic compartments of
1001 microfluidic chambers without rabies virus infection

1002 **Figure supplement 5:** RNA quality assessment and verification of microarray quality
1003 controls

1004 **Table supplement 1:** Membrane properties of uninjured controls vs. axotomized neurons
1005 48 h post-axotomy

1006 **Table supplement 2:** List of transcripts that were significantly changed 24 h after injury.

1007 **Table supplement 3**: Cell-cell adhesion transcripts changed 24 h after injury ($p < 0.1$)

1008

1009